How to cite: *Angew. Chem. Int. Ed.* **2020**, *59*, 14921 – 14926
International Edition: doi.org/10.1002/anie.202004778
German Edition: doi.org/10.1002/ange.202004778

C–H Activation

Fluctuating Storage of the Active Phase in a Mn-Na_2WO_4/SiO_2 Catalyst for the Oxidative Coupling of Methane

*Maximilian J. Werny, Yuanqing Wang, Frank Girgsdies, Robert Schlögl, and Annette Trunschke**

Abstract: *Structural dynamics of a Mn-Na_2WO_4/SiO_2 catalyst were detected directly under reaction conditions during the oxidative coupling of methane via in situ XRD and operando Raman spectroscopy. A new concept of fluctuating storage and release of an active phase in heterogeneous catalysis is proposed that involves the transient generation of active sodium oxide species via a reversible reaction of Na_2WO_4 with Mn_7SiO_{12}. The process is enabled by phase transitions and melting at the high reaction temperatures that are typically applied.*

Introduction

The oxidative coupling of methane (OCM) to ethane and ethene represents an attractive alternative to current crude-oil-based processes in order to access value-added chemicals.[1] Since the pioneering works of Keller and Bhasin,[2] Hinsen and Baerns,[3] and Ito and Lunsford[4] in the early 1980s, the multi-phase Mn-Na_2WO_4/SiO_2 catalyst has established itself as a high-performance system that exhibits extended on-stream stability at high reaction temperatures.[5] Despite extensive investigations, both the active site and working mechanism of the catalyst remain much debated.[6] In general, most research has been directed towards the structural characterization of the catalyst before and after the reaction or in a quenched state.[7] Only limited efforts have, however, been made to elucidate the nature of the catalyst under working conditions.

In this report, a Mn-Na_2WO_4/SiO_2 catalyst (Supporting Information, Table S1, Figures S1–S3), synthesized in large scale by Simon et al.,[5e] was investigated with the aim of identifying structural motifs and phase transitions directly under relevant reaction conditions. A multi-method approach, featuring electron microscopy (SEM-EDX), thermal analysis (TG-DTA-MS), in situ and operando Raman spectroscopy and in situ X-ray diffraction, was adopted. Reference compounds, in form of $Na_2WO_4 \cdot 2H_2O$, $MnWO_4$, and natural braunite (Mn_7SiO_{12})[8] were also examined (Supporting Information, Figures S4–S13). With pure Na_2WO_4 known to undergo a phase transition from solid to liquid at 695 °C (Supporting Information, Figure S11),[9] the formation of a catalytically active liquid component, containing alkali and transition metal oxides, was investigated.

Results and Discussion

The as-synthesized catalyst is a macro-porous material with low specific surface area (2.9 $m^2 g^{-1}$) (Supporting Information, Figure S3). Its crystalline fraction is constituted by α-cristobalite (92 wt%), quartz (0.5 wt%), Na_2WO_4 (4.1 wt%), and mixed-valent Mn_7SiO_{12} (3.4 wt%) (Supporting Information, Figure S1). The manganese silicate mostly contains the transition metal in the oxidation state +3 ($Mn^{2+}Mn^{3+}{}_6SiO_{12}$). Another phase, $MnWO_4$, which only features Mn in the oxidation state +2, was sporadically detected at certain spots by Raman spectroscopy (Figure 1 A, bottom, Supporting Information, Figure S2). By investigating the aforementioned reference compounds using Raman spectroscopy (Supporting Information, Figures S4–S10), all observed bands were successfully allocated for the multi-phase Mn-Na_2WO_4/SiO_2 catalyst system. The low concentration of $MnWO_4$ is expected to arise from the higher stability of Mn_7SiO_{12}, relative to $MnWO_4$, under oxidizing conditions. SEM-EDX revealed an inhomogeneous distribution of manganese, sodium, and tungsten on the catalyst surface and inside the silica support, with Na_2WO_4 preferentially forming separate domains (appearing in yellow-orange in Figure 1 B). Furthermore, large areas of the catalyst are only constituted by manganese, silicon and oxygen. Higher concentrations of Mn, in close vicinity to the Na_2WO_4 phase, may suggest a structural interaction of the Mn-containing phases with Na_2WO_4. Freely existing W can also be observed, suggestive of silica-supported WO_x species. However, typical bands for WO_x species dispersed on silica do not appear in the Raman spectrum of the catalyst (Figure 1 A).[10] Surface inhomogeneities are also reflected in the Raman spectra recorded at different spots, which evidently feature varying concentrations of Na_2WO_4 and Mn_7SiO_{12} (Figure 1 A, top and middle).

After testing the catalyst under relatively mild conditions (Supporting Information, Figure S14), a slightly increased concentration of quartz was observed, yet the general phase composition of the catalyst remained unaltered (Supporting Information, Figure S1). Both the support (in its high-temper-

[*] M. J. Werny, Y. Wang, F. Girgsdies, R. Schlögl, A. Trunschke
Department of Inorganic Chemistry,
Fritz-Haber-Institut der Max-Planck-Gesellschaft
Berlin (Germany)
E-mail: trunschke@fhi-berlin.mpg.de
Y. Wang
BasCat—UniCat BASF Joint Lab, Technische Universität Berlin
(Germany)
Supporting information and the ORCID identification number(s) for the author(s) of this article can be found under:
https://doi.org/10.1002/anie.202004778.

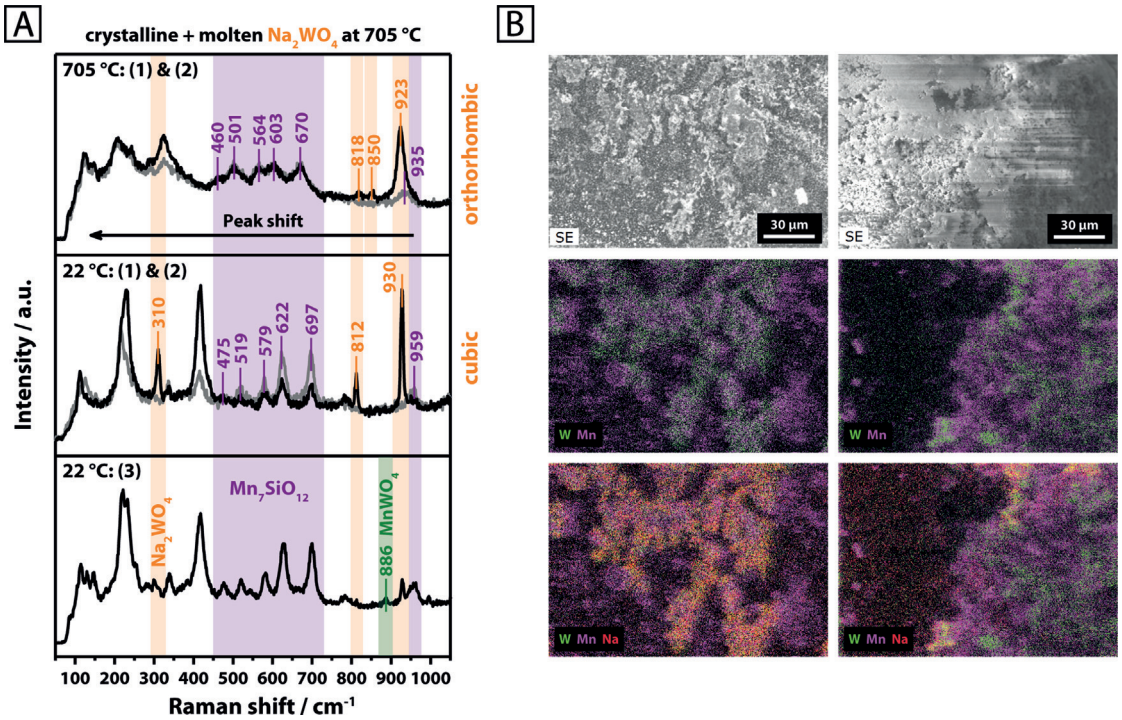

Figure 1. A) Raman spectra of Mn-Na_2WO_4/SiO_2 collected at three different spots using 457 nm excitation, as indicated in brackets, at room temperature (22 °C) and 705 °C in synthetic air ($N_2/O_2 = 79/21$); B) SEM-EDX of two selected areas of the pristine Mn-Na_2WO_4/SiO_2 catalyst surface (Mn: purple, W: green, Na: red).

ature β-cristobalite modification $\vartheta > 225$ °C) as well as the Mn_7SiO_{12} phase did not undergo structural changes in the temperature range of 400–750 °C in synthetic air (Figure 2 A; Supporting Information Figure S15). The Na_2WO_4 phase, on the other hand, displayed significant structural dynamics. When heating to 600 °C, the reflections of cubic Na_2WO_4 were replaced by an unidentified phase that is apparently formed during the transition of cubic to orthorhombic Na_2WO_4 (Figure 2 A; Supporting Information Figure S15). The latter was first observed at 650 °C and subsequently remained stable until 680 °C. Further heating to 690 °C resulted in the complete disappearance of the Na_2WO_4 reflections, which is suggestive of melting. This stands in agreement with the onset melting temperature of pure sodium tungstate ($\vartheta_m = 695$ °C; Supporting Information, Figure S11). An endothermic event, indicated by a DTA signal at 689 °C in the thermal analysis of the catalyst in synthetic air (Supporting Information, Figure S16), further confirms the melting of Na_2WO_4 on the surface of the catalyst support. For the catalyst, the relatively small endothermic signal arises from the low concentration of Na_2WO_4 but is, nevertheless, clearly verified by its reversibility during cooling. Solidification of supported, molten Na_2WO_4 evidently results in the formation of an amorphous phase (Supporting Information, Figure S15). Furthermore, the crystallization of two unidentified phases is observed in the temperature range of 660–600 °C while cubic Na_2WO_4 only reappeared at 450 °C. Similar results were reported by Hou et al.,[6j] who observed a weakening of the reflections for Na_2WO_4 in air from 500 °C onwards and a complete disappearance at 700 °C. In addition to this, a significant broadening of the ν_{sym} (W–O) stretching mode of Na_2WO_4 at 923 cm^{-1} was observed in the Raman spectrum of the catalyst above the melting point of Na_2WO_4 (Figure 1 A, top). Both, Takanabe et al.,[6o] and Yu. et al.,[11] reported similar observations, describing a reversible disappearance and intensity loss of the characteristic Raman bands for Na_2WO_4 supported on TiO_2 and CeO_2, respectively. Raman spectroscopy at different sampling positions clearly proves that the melt does not completely wet the catalyst surface. While in some areas only signals of β-cristobalite and Mn_7SiO_{12} were evident (Figure 1 A, top, gray spectrum), other areas also featured a broadened spectrum of Na_2WO_4 (Figure 1 A, top, black spectrum). In summary, melting of the crystalline Na_2WO_4 phase in the Mn-Na_2WO_4/SiO_2 catalyst was clearly observed in synthetic air by in situ XRD and TG-DTA analysis. However, according to Raman spectroscopy, a full wetting of the catalyst surface with molten Na_2WO_4 does not occur, that is, surface inhomogeneities clearly persist at temperatures higher than 700 °C.

In contrast to this, the structural evolution changes drastically in inert atmosphere. Cubic Na_2WO_4 disappears at 600 °C in favor of an unknown transient phase (Figure 2 B; Supporting Information, Figure S17), which only partially resembles the transient phase formed in air at 600 °C (Figure 2 A). Instead of detecting the formation of orthorhombic Na_2WO_4 at 650 °C, as observed in synthetic air (Figure 2 A), the patterns of the transient peaks are subject to further change. The intensity of the reflection near 33° 2θ, assigned to Mn_7SiO_{12}, starts to decrease, while peaks due to $MnWO_4$ arise (Figure 2 B). The development of the $MnWO_4$ peaks occurs simultaneously with the complete disappearance of the Mn_7SiO_{12} reflection. A significant formation of $MnWO_4$, by reaction of Mn_7SiO_{12} with Na_2WO_4 and/or WO_x, was also evident via Raman spectroscopy for nitrogen feed

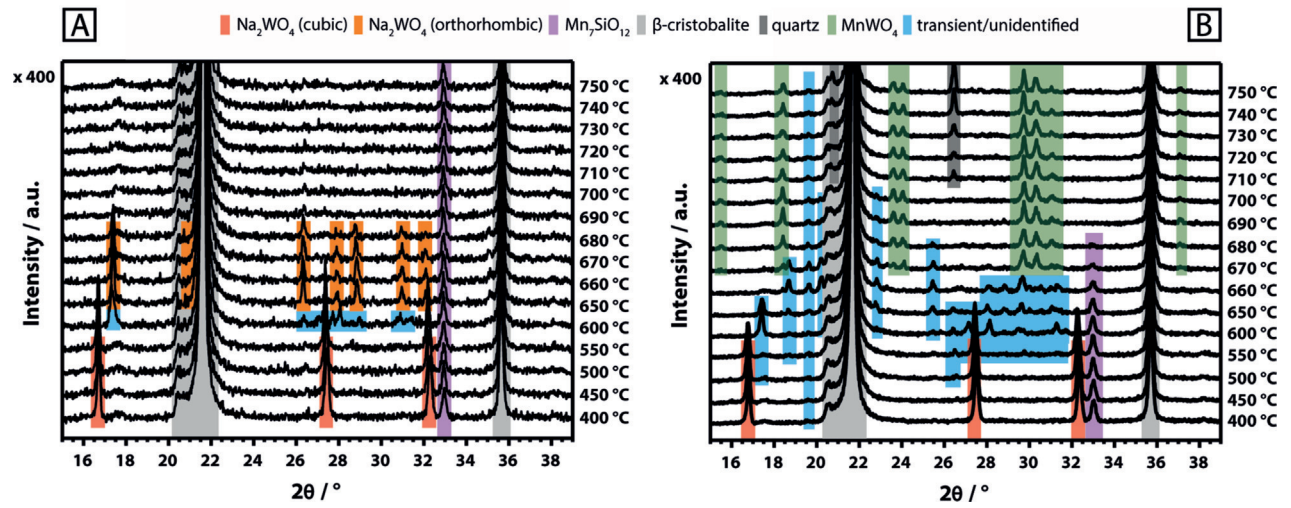

Figure 2. A) In situ XRD of the Mn-Na_2WO_4/SiO_2 catalyst recorded between 400 °C and 750 °C in He/O_2 (He: 17.77 mln min^{-1}, O_2: 2.22 mln min^{-1}); B) In situ XRD of the Mn-Na_2WO_4/SiO_2 catalyst recorded between 400 °C and 750 °C in He (20 mln min^{-1}).

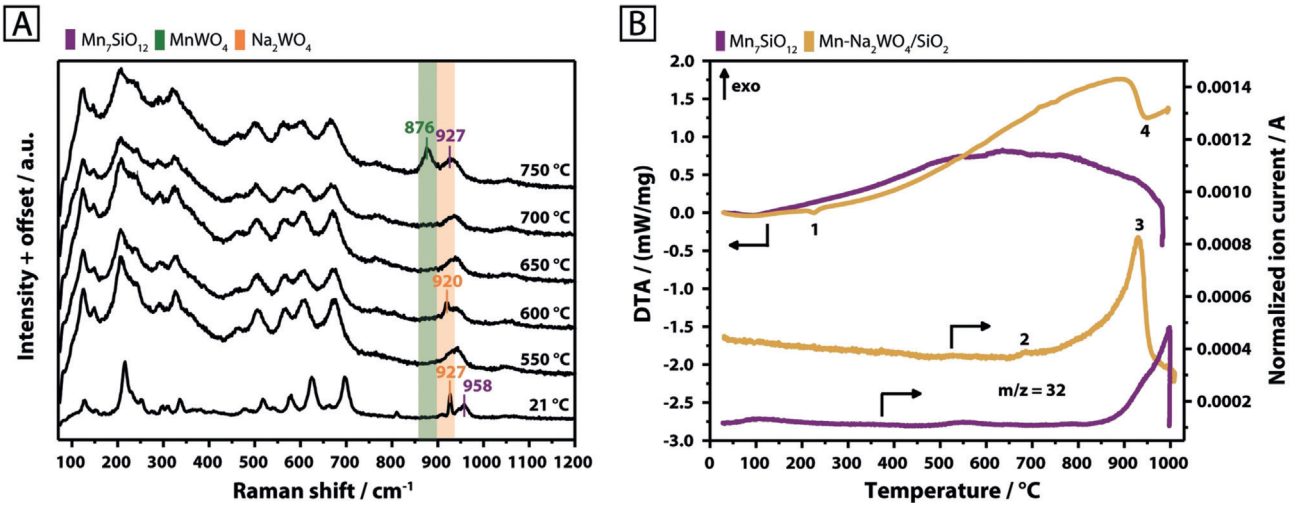

Figure 3. A) In situ Raman spectra of the Mn-Na_2WO_4/SiO_2 catalyst collected at room temperature (21 °C) and between 550 °C and 750 °C in N_2 (20 mln min^{-1}) using 457 nm excitation; B) TG-DTA-MS of the Mn-Na_2WO_4/SiO_2 catalyst (yellow) and Mn_7SiO_{12} (purple) in Ar (70 and 100 mL min^{-1}, respectively). The samples were subjected to a heating rate of 5 °C min^{-1} to reach a maximum temperature of 1000 °C. MS signal intensities were normalized to the carrier gas Ar ($m/z = 40$).

(Figure 3 A). The band of Mn_7SiO_{12} at 958 cm^{-1} is no longer distinguishable at higher temperatures due to shift or broadening of the band of Na_2WO_4 at 927 cm^{-1}. The latter is most likely caused by phase transition and melting of Na_2WO_4 or by formation of tetrahedrally coordinated, silica-supported WO_x species. The disappearance of Mn_7SiO_{12} and cubic Na_2WO_4 in the XRD, starting at 600 °C, is, therefore, most likely connected to a partial or complete conversion of the two phases to $MnWO_4$. Thermal analysis of the Na_2WO_4, $MnWO_4$, and Mn_7SiO_{12} reference compounds (Supporting Information, Figures S11–S13) only revealed a significant oxygen release ($m/z = 32$) at elevated temperatures for the Mn_7SiO_{12} phase, with an onset at 807 °C (Figure 3 B; Supporting Information, Figure S13). Several different thermal events were observed for the Mn-Na_2WO_4/SiO_2 catalyst system in argon (Figure 3 B; Supporting Information, Figure S18). The DTA curve features an endothermic event (1) at 226 °C, which is assigned to the phase transition of the α-cristobalite support to β-cristobalite.[12] Oxygen evolution from the catalyst is shifted to significantly lower temperatures when compared to the Mn_7SiO_{12} reference, with the onset recorded at 653 °C (2). This could be associated with the phase transition of cubic Na_2WO_4 into unknown transient phases at 600 °C, the commencing formation of $MnWO_4$ at 650 °C as well as the disappearance of Mn_7SiO_{12}, also observed from 650 °C onwards (Figure 2 B). Instead of a well-defined endothermic peak, the DTA curve only displays minor irregularities in the temperature regime between 600 °C and 700 °C (Figure 3 B; Supporting Information, Figure S18). It is possible that the superposition of the melting and redox processes, as observed via in situ XRD in the absence of air in this temperature range, limits the ability of DTA to clearly detect melting.

Progressive surface mobility, initiated by restructuring of supported Na_2WO_4 above 600 °C and facilitated by melting of residual Na_2WO_4 at higher temperatures, can enable the reaction between Mn_7SiO_{12} and Na_2WO_4 as shown in

Equation (1). This, in turn, leads to the reduction of Mn^{3+} (in Mn_7SiO_{12}) to Mn^{2+} (in $MnWO_4$), the release of molecular oxygen with its maximum at 927 °C ((3) and (4) in Figure 3B), and the formation of amorphous or dispersed sodium oxide.

$$Mn^{2+}Mn^{3+}{}_6SiO_{12} + 7\,Na_2WO_4 \leftrightarrow 7\,MnWO_4 + 7\,Na_2O + SiO_2 + 1.5\,O_2 \quad (1)$$

The broad temperature range for the oxygen release covers the onset temperature of oxidative coupling of methane (650 °C) as well as the reaction temperatures that are typically applied (700–800 °C). A weight loss of 0.2 % (0.22 mg) was caused by the event, with the DTA curve indicating endothermicity (4). It is postulated that the process described in Equation (1) provides mobile lattice oxygen under steady-state operation of the catalyst. This is in agreement with O_2-TPD experiments performed by Gordienko et al.,[13] who identified two forms of lattice oxygen that may potentially contribute to catalysis upon desorption at relevant temperatures. The source of oxygen has been attributed to manganese oxide,[6j,7] or any unspecified lattice oxygen.[14] Potentially more decisive is the release of an active form of sodium oxide species that has been proposed to catalyse the oxidative coupling of methane by generation of OH radicals at high temperatures,[6l,m,o] presumably under involvement of homogeneous gas-phase reactions[15] due to the high volatility of sodium compounds under operation conditions.[16]

Evidence, that the redox process described in Equation (1) occurs under reaction conditions and is indeed reversible, was provided by operando Raman spectroscopy at different reaction temperatures and feed compositions (Figure 4; Supporting Information Figure S19). In all operando spectra (Figures 4A and B), the region of 100–400 cm^{-1} is dominated by a broad band of the β-cristobalite support, which is formed via phase transition from α-cristobalite at 225 °C.[12a,c,17] The spectra recorded under steady-state conditions in a $CH_4/O_2/N_2$ (4:1:4) feed at various temperatures (Figure 4A) predominantly feature bands of β-cristobalite and the remaining steady-state concentrations of Mn_7SiO_{12} (450–700 cm^{-1}) and Na_2WO_4 (920–930 cm^{-1}). At the highest reaction temperature, the formation of $MnWO_4$ becomes apparent, as indicated by a very weak band at 874 cm^{-1}. Carbon oxides, ethane, and water were identified as the main reaction products via online mass spectrometry and gas chromatography in the effluent gas of the Raman cell (Supporting Information, Figures S20,S21). Significant formation of coke was not observed (Figure 4A). The selectivity to C_{2+} products was much lower compared to analogous experiments conducted in a quartz fixed bed reactor without dilution of the catalyst (Supporting Information, Figure S14), which is attributed to consecutive reactions of the desired C_{2+} products on the hot stainless-steel walls of the operando cell and the inadequate reactor geometry. However, comparison of the catalytic tests conducted with the empty operando cell and the same cell filled with the catalyst under identical reaction conditions clearly showed a lower activity and selectivity to C_{2+} products for the empty reactor (Figure 4C).

Changes to the spectral composition were observed upon switching to a reducing CH_4/N_2 (4:5) feed at 700 °C (Figure 4B). This was accompanied by a significant decline in catalyst performance and the formation of hydrogen and carbon monoxide as main products, suggesting that lattice oxygen is consumed and gas-phase reactions as well as methane pyrolysis prevail under these conditions (Supporting Information, Figures S20 and Figure S21). The complete removal of oxygen leads to the formation of $MnWO_4$, as indicated by the band at 878 cm^{-1} (Figures 4B and D). Thus, a reaction of Na_2WO_4 and/or WO_x with Mn_7SiO_{12} and/or MnO_x to yield $MnWO_4$ occurs under reducing conditions. The formation of coke is excluded here based on Raman spectroscopy (Figure 4A). During catalyst regeneration using the initial reaction feed ($CH_4/O_2/N_2 = 4:1:4$), braunite is suddenly reformed at the expense of $MnWO_4$ after approximately 8 h (Figure 4D). Moreover, due to this reversible phase transformation, the formation of C_2 products is reinitiated (Supporting Information, Figure S20 and Figure S21 after 8 h), thereby highlighting the significance of the Mn_7SiO_{12} phase in maintaining catalytic activity. The presence of Mn_7SiO_{12} is also clearly responsible for the formation of CO_2 in place of CO (Supporting Information, Figure S21). As can be seen in Figure 4A, the spectrum initially observed under steady-state conditions, is restored entirely by switching back to a $CH_4/O_2/N_2$ feed (Figure 4A, red spectrum).

Conclusion

In conclusion, the present in situ and operando experiments disclosed reversible redox activity of the Mn_7SiO_{12}, $MnWO_4$, and Na_2WO_4 phases under operation conditions in the oxidative coupling of methane over Mn-Na_2WO_4/SiO_2. A new concept is proposed that involves the fluctuating storage and release of an active phase in heterogeneous catalysis. According to Equation (1), active sodium oxide species, which are responsible for high activity and selectivity in the oxidative coupling of methane,[6o] are generated in the catalytically relevant temperature regime in small amounts. The extent of this reaction is controlled by the oxygen partial pressure in the gas phase and the redox chemistry on the surface (Scheme 1). While the structural synergy of all phases is responsible for the high stability and activity of the catalyst, the supported Na_2WO_4 phase acts as storage phase responsible for transient generation of active sodium oxide species that would, in absence of the stabilizing Mn_7SiO_{12}–$MnWO_4$ redox couple, suffer from steady sublimation,[16] thus leading to catalyst deactivation.[6b,g] As long as the oxygen partial pressure in the reactor is not too low, a small steady-state concentration of the active phase is formed according to Scheme 1.

Phase transitions and melting of Na_2WO_4 enable the generation of the active phase by providing mobile sodium species. Furthermore, the supported Mn_7SiO_{12} phase was observed to function as oxygen-donor at working temperatures, which further enhances sodium oxide formation and, thus, has implications for the reactivity. However, the availability of adsorbed or lattice oxygen due to the presence of

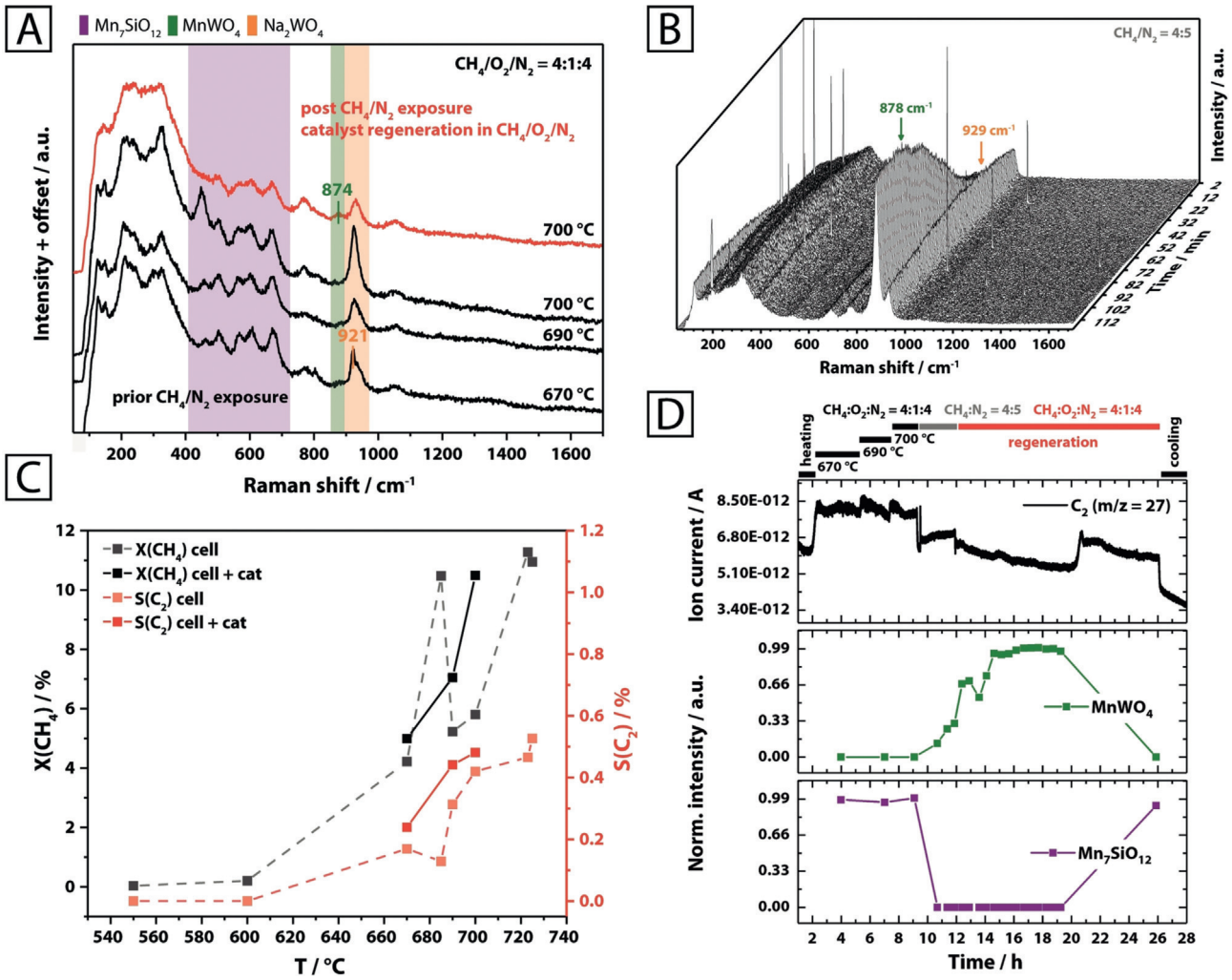

Figure 4. Operando Raman experiment conducted on the Mn-Na_2WO_4/SiO_2 catalyst using 457 nm excitation. The catalyst was studied in a temperature range of 670–700 °C under $CH_4/O_2/N_2 = 4:1:4$ (A, black spectra), followed by exposure to $CH_4/N_2 = 4:5$ at 700 °C (B) and subsequent regeneration under $CH_4/O_2/N_2 = 4:1:4$ at 700 °C (A, red spectrum) (total flow = 10 mL min^{-1}; W/F = 0.0030 g min mL^{-1}). The Raman spectra under steady-state conditions (A) were collected using an exposure time of 30 min. $X(CH_4)$ and $S(C_2)$ indicate that the catalyst was active in the given temperature regime (C). By comparing the collected mass spectrometry data that is representative for C_2 formation and the band intensities for Mn_7SiO_{12} (670 cm^{-1}) and $MnWO_4$ (878 cm^{-1}), the re-formation of Mn_7SiO_{12} from $MnWO_4$ was found to be associated with an increase in catalytic activity during the catalyst regeneration phase.

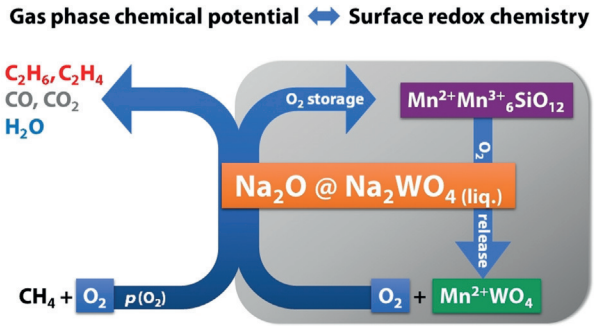

Scheme 1. Impeded phase transition: Transient release of the active phase controlled by the partial pressure of oxygen in the gas phase and the surface redox chemistry.

redox-active elements alone[6j,7,13,14] cannot be responsible for the outstanding performance of the Mn-Na_2WO_4/SiO_2 catalyst and does not explain the mechanistic role and importance of Na in this system. On the other hand, a pure silica-supported sodium oxide would rapidly deactivate under the severe reaction conditions applied in the oxidative coupling of methane.[6g] Only the chemical complexity of the Mn-Na_2WO_4/SiO_2 catalyst guarantees long-term stability. The synergistic element combination discovered by chance is so successful because melting and redox reactions occur in the same temperature window (Figure 2 and Figure 3).

In the presence of gas-phase oxygen, the phase transition of Mn_7SiO_{12} and Na_2WO_4 into Na_2O and $MnWO_4$ [Eq. (1)] is largely impeded and generates only transient amounts of active[6o] sodium oxide species. Apparently, only a small concentration of oxygen is necessary to keep the system in this highly active state (> 88 % oxygen conversion in the steady state, see Supporting Information, Figure S21, $t > 8$ h). Such a low concentration of oxygen in the gas phase is beneficial in terms of the selectivity. Only in total absence of oxygen is the system disturbed and $MnWO_4$ formed in

noticeable amounts. The oxygen donor Mn_7SiO_{12} (Figure 3B), however, evidently hinders a complete and rapid transformation into $MnWO_4$ and Na_2O (Figure 4B), which would lead to a loss of Na_2O due to sublimation and progressive catalyst deactivation. The described scenario may also be considered as displacement of the redox chemistry from the organic to the inorganic part of the hybrid reaction system. Therefore, in future concepts of catalyst design it might be reasonable to take into account that the activation of methane could also proceed via an acid-base reaction by using the strong base O^{2-} as catalyst avoiding radical chemistry in the selective pathway.

Our experiments clearly show that $MnWO_4$ is a product of catalyst deactivation, which is formed under strongly reducing reaction conditions. However, regeneration by increasing the partial pressure of oxygen in the feed again is possible (Figures 4D and Supporting Information, Figure S21).

The study in this report is an example for how in situ and operando Raman spectroscopy techniques can be applied as effective, non-invasive tools to obtain valuable information on high-temperature catalysts under relevant operation conditions. Based on experimental evidence, it is clearly explained how the chemical complexity of the Mn-Na_2WO_4/SiO_2 catalyst warrants a high yield of C_2 products and long-term stability in the oxidative coupling of methane.

Acknowledgements

Our sincere gratitude goes to Ulla Simon (TU Berlin) for synthesizing the Mn-Na_2WO_4/SiO_2 catalyst that was used in this study. We would also like to thank Wiebke Frandsen, Dr. Thomas Lunkenbein, Dr. Milivoj Plodinec, Jasmin Allan, Dr. Andrey Tarasov, Dr. Olaf Timpe, Maike Hashagen, Dr. Pierre Kube, Dr. Hamideh Ahi and Sven Richter for their technical assistance and scientific discussions. Finally, we would like to extend our appreciation towards Dr. Rupert Hochleitner of the Mineralogische Staatssammlung München as well as the Naturkundemuseum Berlin for providing specimens of natural braunite (Mn_7SiO_{12}).

Conflict of interest

The authors declare no conflict of interest.

Keywords: catalysis · C—H activation · OCM · operando analysis · Raman spectroscopy

[1] a) J. H. Lunsford, *Catal. Today* **2000**, *63*, 165 – 174; b) P. F. van den Oosterkamp, *Encyclopedia of Catalyis*, *Vol. 6*, Wiley-VCH, Weinheim, **2003**; c) E. McFarland, *Science* **2012**, *338*, 340 – 342; d) P. Schwach, X. Pan, X. Bao, *Chem. Rev.* **2017**, *117*, 8497 – 8520.
[2] G. E. Keller, M. M. Bhasin, *J. Catal.* **1982**, *73*, 9 – 19.
[3] W. Hinsen, M. Baerns, *Chem. Ztg.* **1983**, *107*, 223 – 226.
[4] T. Ito, J. H. Lunsford, *Nature* **1985**, *314*, 721.
[5] a) J. Lin, J. Gu, D. Yang, C. Zhang, Y. Yang, Y. Chu, S. Li, *Shiyou Huagong* **1995**, *24*, 293 – 298; b) X. L. Wang, J. N. Zhang, D. X. Yang, C. W. Zhang, J. Z. Lin, S. B. Li, *Shiyou Huagong* **1997**, *26*, 361 – 367; c) S. Pak, P. Qiu, J. H. Lunsford, *J. Catal.* **1998**, *179*, 222 – 230; d) H. Liu, X. Wang, D. Yang, R. Gao, Z. Wang, J. Yang, *J. Nat. Gas Chem.* **2008**, *17*, 59 – 63; e) U. Simon, O. Görke, A. Berthold, S. Arndt, R. Schomäcker, H. Schubert, *Chem. Eng. J.* **2011**, *168*, 1352 – 1359; f) S. Arndt, T. Otremba, U. Simon, M. Yildiz, H. Schubert, R. Schomäcker, *Appl. Catal. A* **2012**, *425 – 426*, 53 – 61.
[6] a) Z. C. Jiang, C. J. Yu, X. P. Fang, S. B. Li, H. L. Wang, *J. Phys. Chem.* **1993**, *97*, 12870 – 12875; b) D. J. Wang, M. P. Rosynek, J. H. Lunsford, *J. Catal.* **1995**, *155*, 390 – 402; c) J. Wu, S. Li, *J. Phys. Chem.* **1995**, *99*, 4566 – 4568; d) Z. C. Jiang, H. Gong, S. B. Li, *Stud. Surf. Sci. Catal.* **1997**, *112*, 481 – 490; e) A. Palermo, J. P. Holgado Vazquez, A. F. Lee, M. S. Tikhov, R. M. Lambert, *J. Catal.* **1998**, *177*, 259 – 266; f) Y. Kou, B. Zhang, J.-z. Niu, S.-b. Li, H.-l. Wang, T. Tanaka, S. Yoshida, *J. Catal.* **1998**, *173*, 399 – 408; g) A. Palermo, J. P. Holgado Vazquez, R. M. Lambert, *Catal. Lett.* **2000**, *68*, 191 – 196; h) A. Malekzadeh, A. Khodadadi, M. Abedini, M. Amini, A. Bahramian, A. K. Dalai, *Catal. Commun.* **2001**, *2*, 241 – 247; i) S.-f. Ji, T.-c. Xiao, S.-b. Li, C.-z. Xu, R.-l. Hou, K. S. Coleman, M. L. H. Green, *Appl. Catal. A* **2002**, *225*, 271 – 284; j) S. Hou, Y. Cao, W. Xiong, H. Liu, Y. Kou, *Ind. Eng. Chem. Res.* **2006**, *45*, 7077 – 7083; k) V. Salehoun, A. Khodadadi, Y. Mortazavi, A. Talebizadeh, *Chem. Eng. Sci.* **2008**, *63*, 4910 – 4916; l) K. Takanabe, E. Iglesia, *Angew. Chem. Int. Ed.* **2008**, *47*, 7689 – 7693; *Angew. Chem.* **2008**, *120*, 7803 – 7807; m) K. Takanabe, E. Iglesia, *J. Phys. Chem. C* **2009**, *113*, 10131 – 10145; n) K. Takanabe, *J. Jpn. Pet. Inst.* **2012**, *55*, 1 – 12; o) K. Takanabe, A. M. Khan, Y. Tang, L. Nguyen, A. Ziani, B. W. Jacobs, A. M. Elbaz, S. M. Sarathy, F. F. Tao, *Angew. Chem. Int. Ed.* **2017**, *56*, 10403 – 10407; *Angew. Chem.* **2017**, *129*, 10539 – 10543; p) D. Kiani, S. Sourav, J. Baltrusaitis, I. E. Wachs, *ACS Catal.* **2019**, *9*, 5912 – 5928.
[7] M. Sinev, E. Ponomareva, I. Sinev, V. Lomonosov, Y. Gordienko, Z. Fattakhova, D. Shashkin, *Catal. Today* **2019**, *333*, 36 – 46.
[8] R. Hochleitner, natural mineral braunite, Langban, Sweden ed., Mineralogische Staatssammlung München.
[9] a) R. W. Goranson, F. C. Kracek, *J. Chem. Phys.* **1935**, *3*, 87 – 92; b) P. H. Bottelberghs, F. R. van Buren, *J. Solid State Chem.* **1975**, *13*, 182 – 191; c) K. G. Bramnik, H. Ehrenberg, *Z. Anorg. Allg. Chem.* **2004**, *630*, 1336 – 1341; d) K. D. Singh Mudher, M. Keskar, K. Krishnan, V. Venugopal, *J. Alloys Compd.* **2005**, *396*, 275 – 279.
[10] S. Lwin, Y. Li, A. I. Frenkel, I. E. Wachs, *ACS Catal.* **2016**, *6*, 3061 – 3071.
[11] Z. Q. Yu, X. M. Yang, J. H. Lunsford, M. P. Rosynek, *J. Catal.* **1995**, *154*, 163 – 173.
[12] a) J. B. Bates, *J. Chem. Phys.* **1972**, *57*, 4042 – 4047; b) D. M. Hatch, S. Ghose, *Phys. Chem. Miner.* **1991**, *17*, 554 – 562; c) I. P. Swainson, M. T. Dove, D. C. Palmer, *Phys. Chem. Miner.* **2003**, *30*, 353 – 365.
[13] Y. Gordienko, T. Usmanov, V. Bychkov, V. Lomonosov, Z. Fattakhova, Y. Tulenin, D. Shashkin, M. Sinev, *Catal. Today* **2016**, *278*, 127 – 134.
[14] V. Fleischer, R. Steuer, S. Parishan, R. Schomäcker, *J. Catal.* **2016**, *341*, 91 – 103.
[15] S. Ruf, G. Emig, *J. Mol. Catal. A* **1999**, *146*, 271 – 278.
[16] D. L. Hildenbrand, K. H. Lau, *J. Chem. Phys.* **1993**, *98*, 4076 – 4081.
[17] P. Richet, B. O. Mysen, *Geophys. Res. Lett.* **1999**, *26*, 2283 – 2286.

Manuscript received: April 1, 2020
Accepted manuscript online: May 4, 2020
Version of record online: June 17, 2020

